

The Tilt of Mean Dynamic Topography and its Seasonality Along the Coast of the Chinese Mainland

 Wenqiang Lin¹ , Hongyang Lin^{1,2} , and Jianyu Hu^{1,2} 
¹State Key Laboratory of Marine Environmental Science, College of Ocean and Earth Sciences, Xiamen University, Xiamen, China, ²Southern Marine Science and Engineering Guangdong Laboratory (Zhuhai), Zhuhai, China

Key Points:

- Estimates of Chinese coastal MDT tilt from geodetic and ocean approaches agree with each other
- The Chinese coastal MDT shows an overall northward drop and an evident seasonality with steeper tilt in winter and flatter tilt in summer
- The tilt is induced by wind stress in winter and by open-ocean forcing (i.e., Kuroshio) in summer

Correspondence to:

 H. Lin and J. Hu,
hylin@xmu.edu.cn;
hujy@xmu.edu.cn

Citation:

 Lin, W., Lin, H., & Hu, J. (2021). The tilt of mean dynamic topography and its seasonality along the coast of the Chinese mainland. *Journal of Geophysical Research: Oceans*, 126, e2020JC016778. <https://doi.org/10.1029/2020JC016778>

Received 8 SEP 2020

Accepted 18 DEC 2020

Abstract Tilt of coastal mean dynamic topography (MDT) has recently been investigated in many regions, but few studies have examined the seasonality of the MDT along the coast of the Chinese mainland. The China seas are relatively unique as they experience prominent seasonal changes in monsoons and the China Coastal Currents, which are supposed to affect the coastal MDT significantly. This study investigates the Chinese coastal MDT tilt and its seasonality based on the geodetic and ocean approaches. The two independent approaches show a good agreement in their respective estimates. The Chinese coastal MDT presents an overall northward drop and undergoes an evident seasonality with steeper slopes in winter and flatter ones in summer. A dynamical analysis based on alongshore momentum equation suggests that the alongshore MDT along the coast of the Chinese mainland is a counter balance of contributions from the alongshore wind and the coastal current-induced bottom friction, with both of them having prominent seasonality. The overall northward drop is in fact induced primarily by the strong alongshore wind stress in winter and by coastal currents in summer, in particular for the segment between Xiamen and Zhapo. The wintertime coastal MDT is well predicted by the arrested topographic wave model, which however could not reproduce the summertime tilt. The summertime MDT is more likely affected by the open-ocean forcing (i.e., the latitudinal difference of the Kuroshio strength) and a return flow caused by flattening the coastal tilt piled up by the previous winter monsoon.

Plain Language Summary The mean dynamic topography (MDT) is the height of mean sea surface above the geoid, an idealized surface the ocean would take under the influence of gravity and Earth rotation alone. The deviation of MDT is due to the existence of external forcing such as winds, currents, etc. The geostrophic balance (between the MDT tilt and Coriolis force) breaks down at the coast because no flow could penetrate the solid boundary. Hence, the coastal MDT dynamics have attracted increasing attention in recent years. A number of studies have examined the features and dynamics of coastal MDT tilt along many coasts in the world, but few have examined the seasonality of coastal MDT tilt or focused on the Chinese coastline. Our study investigates the MDT tilt along the Chinese coast based on two independent approaches. The results show that the MDT is high in the southern part and low in the northern part of the Chinese coast. Such a northward drop feature is found all year round but it is steeper in winter than in summer. The wintertime coastal MDT is controlled by the strong monsoon winds, while the summertime coastal MDT is more related to the open-ocean and local currents.

1. Introduction

Tilt of the mean dynamic topography (MDT) is to first-order balanced by the Coriolis force in the deep ocean. The geostrophy, however, breaks down at the coast due to the no normal flow condition, which leads to fundamentally different dynamics governing the alongshore MDT. There have been a growing number of studies in estimating the tilt of coastal MDT and their governing dynamics in recent years (e.g., Higginson et al., 2015; Huang, 2017; Kuroishi, 2013; Lin et al., 2015; Woodworth et al., 2012). Two approaches are often used in these studies to estimate the coastal MDT. The geodetic approach incorporates tidal gauge and Global Positioning System (GPS) measurements to obtain the mean sea surface referenced to the reference ellipsoid and then to the geoid (i.e., MDT) with the aid of a geoid model. The ocean approach directly uses output from an ocean model of which the sea level, to a good approximation, has already been referenced to the geoid. Close agreement between the two independent approaches in the estimation of coastal MDT has been found in many previous studies (e.g., Higginson et al., 2015; Lin et al., 2015; Woodworth et al., 2012), thereby allowing investigators to use model output to diagnose the dynamics.

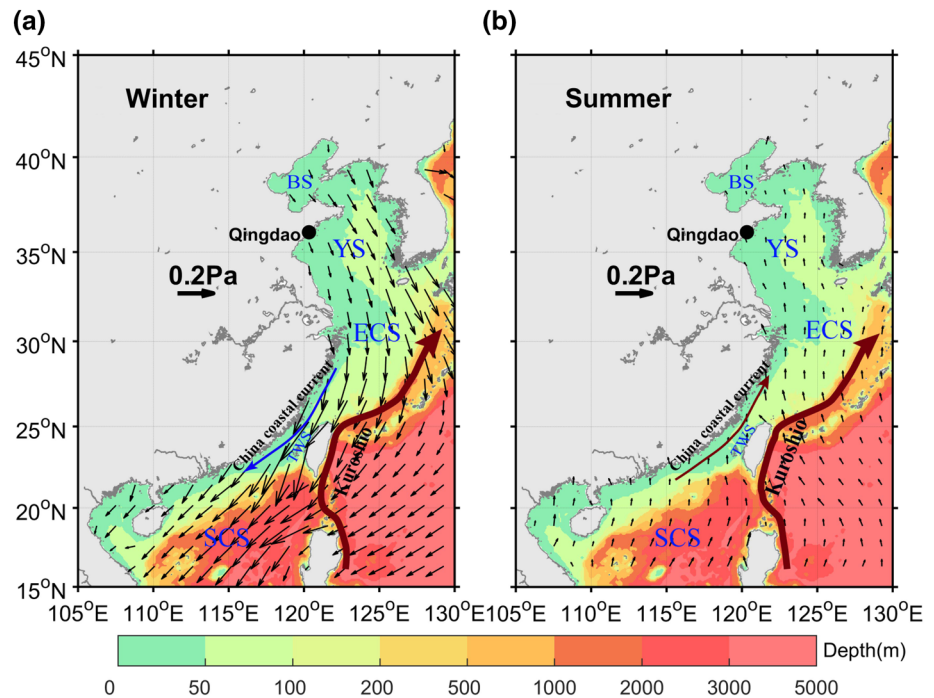


Figure 1. Schematic map of wind stress (vectors, in Pa) and the China Coastal Current in the China seas in (a) winter and (b) summer. The color shading shows the bathymetry (in m). The wind stress is from hourly National Center for Environmental Prediction (NCEP) Climate Forecast System Reanalysis (CFRSR). The bold carmine arrow indicates the pathway of the Kuroshio. The black dot indicates the location of Qingdao tide gauge. BS, YS, ECS, TWS, and SCS denote the Bohai Sea, Yellow Sea, East China Sea, Taiwan Strait, and South China Sea, respectively.

Tilt of alongshore coastal MDT has been examined in many regions of the World Ocean, including the Atlantic coast of North America (e.g., Higginson et al., 2015; Xu & Oey, 2011), Pacific coast of North America and Japan (Lin et al., 2015), Australian coast (Featherstone & Filmer, 2012), British coast (Penna et al., 2013), or a combination of them (e.g., Sturges, 1974; Woodworth et al., 2012). However, few studies have examined the tilt of coastal MDT along the coastline of the Chinese mainland. There were two previous studies tackling this problem by using tide-gauge observations (Zhai et al., 1993; Zhao & Han, 1990), but these studies fall short either in applying unrealistic assumptions or in the lack of dynamical interpretations. Based on tide gauge, altimetry and steric measurements, Zhang (2002) demonstrated the existence of a sea-level slope along the Chinese coast, and suggested that the tilt is associated with the coastal currents and offshore circulation, which are affected by the subsurface density structure, atmospheric forcing, wave breaking, and topography. Although possible factors were speculated, detailed dynamical analysis was lacking in Zhang (2002).

Compared to the abovementioned regions, one of the unique features in the China seas is that they experience monsoons with prominent seasonal changes in wind magnitude and direction (shown schematically in Figure 1). In winter, the China seas are predominantly forced by northeasterly or northerly winds (Figure 1a). In summer, southwesterly and southerly winds blow in the South China Sea and the southern Taiwan Strait, while southerly and southeasterly winds blow in the northern Taiwan Strait, the East China Sea, the Yellow Sea, and the Bohai Sea (Figure 1b; e.g., Chen et al., 2014; Hu & Wang, 2016; Lau & Li, 1984; Tomczak & Godfrey, 1994). Associated with the seasonally reversed monsoonal winds, the China Coastal Currents also have the evident seasonality in both magnitude and direction (Naimie et al., 2001), which could potentially affect the alongshore MDT tilt. The seasonality of coastal MDT tilt has been examined in other regions of the World Ocean. For example, Hickey and Pola (1983) used monthly mean sea level data, by adding the long-term mean steric data of Reid and Mantyla (1976), to obtain the seasonal oscillation of sea-level slope along the west coast of the United States. Along the west coast of the United States, Werner and Hickey (1983) and McCabe et al. (2015) suggested that the seasonal variations of the large-scale

along-shelf sea-level slope were consistent with the cross-shelf flow structure. Nevertheless, the physical processes of circulation on the continental shelf are different for different shelves and vary with season (Stommel & Leetmaa, 1972). Therefore, in addition to the annual mean coastal MDT tilt, it is of great interest to investigate the seasonal changes of MDT tilt along the coast of the Chinese mainland.

The manuscript is organized as follows. Section 2 describes the data and approaches used to estimate the MDT along the coast of the Chinese mainland. Quantitative comparison and seasonal variations of the tilts are presented in Section 3, and a momentum diagnosis is provided in Section 4. Section 5 discusses the dynamical mechanisms that could potentially interpret the coastal MDT. The results are summarized in Section 6.

2. Data and Methods

Following previous studies, we estimate the Chinese coastal MDT based on the geodetic and ocean approaches. Due to the lack of GPS data, we are unable to obtain the mean sea surface referenced to the geoid for Chinese tide gauge stations. Instead, we level the mean sea surface at each tide gauge station to the leveling system of Chinese National Height Datum 1985 (NHD85). NHD85 takes the mean sea surface at Qingdao tide gauge over the period 1952–1979 as the zero point, which also serves as the datum for all other tide gauges in China. The height difference between the local benchmark of a tide gauge and the Qingdao datum could be obtained via the differential spirit leveling. Therefore, NHD85 is regarded as an equipotential surface that is parallel to the geoid up to an offset. We can thus estimate the tilt of MDT along the Chinese coast based on this NHD85 system without using the GPS data. An important question is to what extent can we assume that NHD85 is an equipotential surface. According to Feng et al. (1998), the error of leveling can be estimated by $\pm 1.5\sqrt{L}$ mm, where L is the leveling distance in km. Suppose the leveling distance between Qingdao and Shanwei is about $L = 3,000$ km, then the transmission error is about ± 0.08 m (Zhang, 2002), which is much smaller than the MDT difference between the Bohai Sea and South China Sea (about 0.75 m; Figure 2). We have managed to obtain convergent estimates of coastal MDT from the two independent approaches (detailed in Section 3), giving us confidence to consider our above assumption as broadly valid.

2.1. Geodetic Approach

The locations of eight tide gauge stations along the coast of the Chinese mainland are shown in Figure 2b. Monthly tide gauge data over the period of October 1992 to September 1994 were obtained from the Revised Local Reference (RLR) data set of the Permanent Service for Mean Sea Level (PSMSL) (Higginson et al., 2015; Woodworth & Player, 2003), with the mean sea surface at each tide gauge referenced to a local benchmark. Most of the tide gauge benchmarks along the coast of the Chinese mainland have been leveled to the NHD85 system. Four tide gauge stations are discarded because of the lack of transformation relation between RLR and NHD85. Some of the benchmark transformation relationships can be obtained through the website of the Global Sea Level Observing System (<https://www.gloss-sealevel.org/gloss/gloss-station-handbook>) (the bold number in Table 1), and the others can be gained from historical studies (e.g., Yu et al., 1989) (regular number in Table 1).

2.2. Ocean Approach

The ocean approach estimates the coastal MDT based on the sea surface height output from the Hybrid Coordinate Ocean Model (HYCOM) incorporating the Navy Coupled Ocean Data Assimilation (NCODA) system (Cummings & Smedstad, 2013). This model assimilates available satellite altimeter observations, in-situ sea surface temperature, and available temperature and salinity profiles from XBTs, Argo floats, and moored buoys. The model output has been proven to be in closest agreement, among a list of 11 ocean models, with the geodetic estimates of coastal tilt along the east coast of North America (Higginson et al., 2015). In addition, this model output has been extensively used in the China seas and proven to perform well in reproducing many features in, e.g., the South China Sea (e.g., Gordon et al., 2012; Park & Farmer, 2013), the East China Sea (e.g., Jia et al., 2013; Yu et al., 2015), and the Yellow Sea (e.g., Yang et al., 2019).

The HYCOM product we use is the Global Ocean Forecasting System 3.0 (GOFS 3.0): HYCOM + NCODA Global 1/12° Reanalysis data. It contains daily and 3-hourly global analysis fields with a horizontal

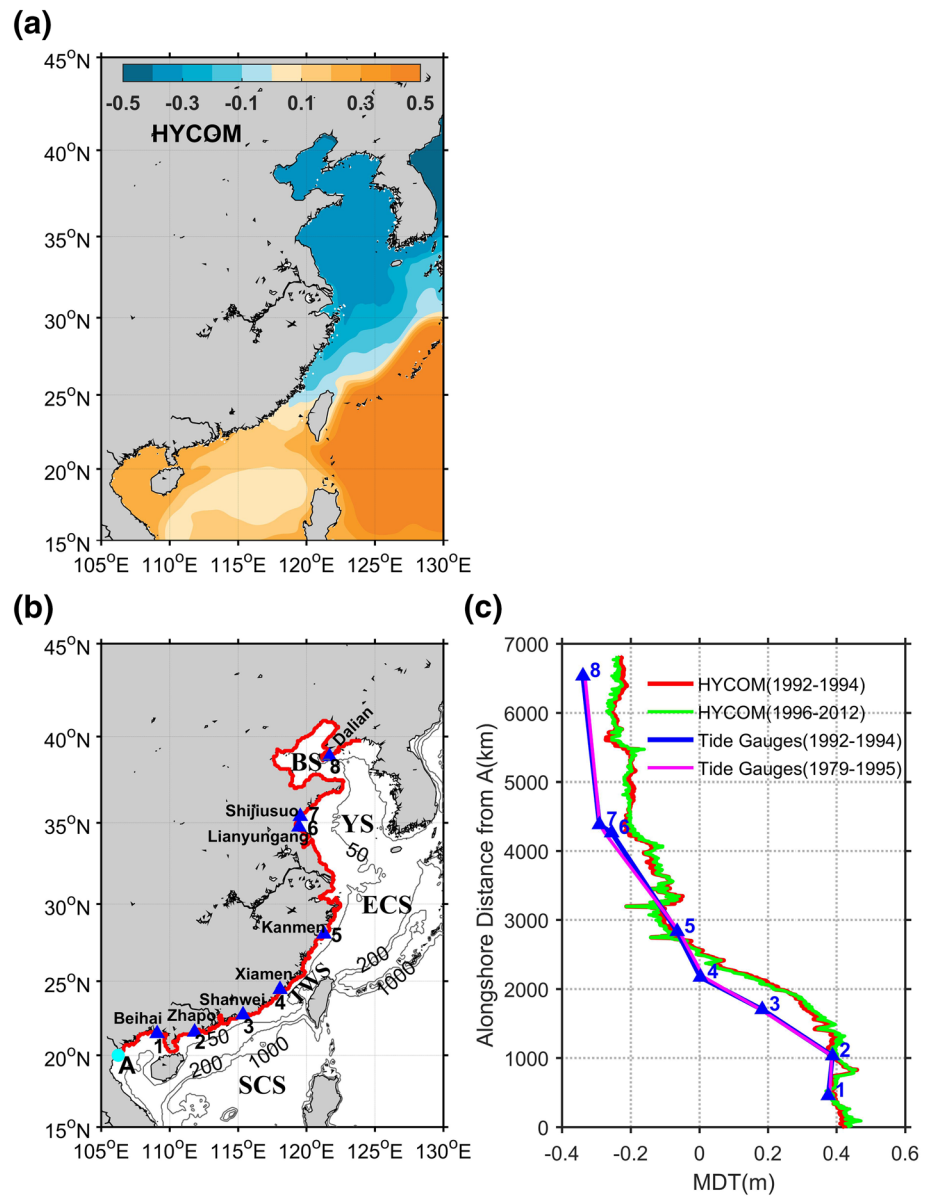


Figure 2. (a) Annual MDT (in m) from HYCOM for the period of October 1992 to September 1994. (b) Location of the eight tide gauge stations (blue markers with the name and respective number labeled) and map of the China seas. The red line shows the coast of the Chinese mainland where the coastal MDT from the model will be used. Gray lines indicate the 50, 200, and 1,000 m isobaths. The cyan point A in (b) denotes the beginning point of the coastline. (c) The annual coastal MDT estimates from HYCOM (red line: 1992–1994; green line: 1996–2012) to tide gauges (blue line: 1992–1994; magenta line: 1979–1995). MDT, mean dynamic topography; HYCOM, HYBRID Coordinate Ocean Model.

resolution of $1/12^\circ$ and 32 vertical layers. The topography is derived from the 30-arc sec GEBCO data set, which is interpolated by the Naval Research Laboratory to a uniform $0.08^\circ \times 0.08^\circ$ grid between 80.48°S and 80.48°N . The model was initialized using wind stress, wind speed, heat flux, and precipitation from the

Table 1
The Benchmark Height Difference (in mm) Between RLR and the NHD85 System

Stations	Dalian	Shijiusuo	Lianyungang	Kanmen	Xiamen	Shanwei	Zhapo	Beihai
NHD85-RLR	7,081	7,015	6,917	6,742	6,693	6,550	6,285	6,291

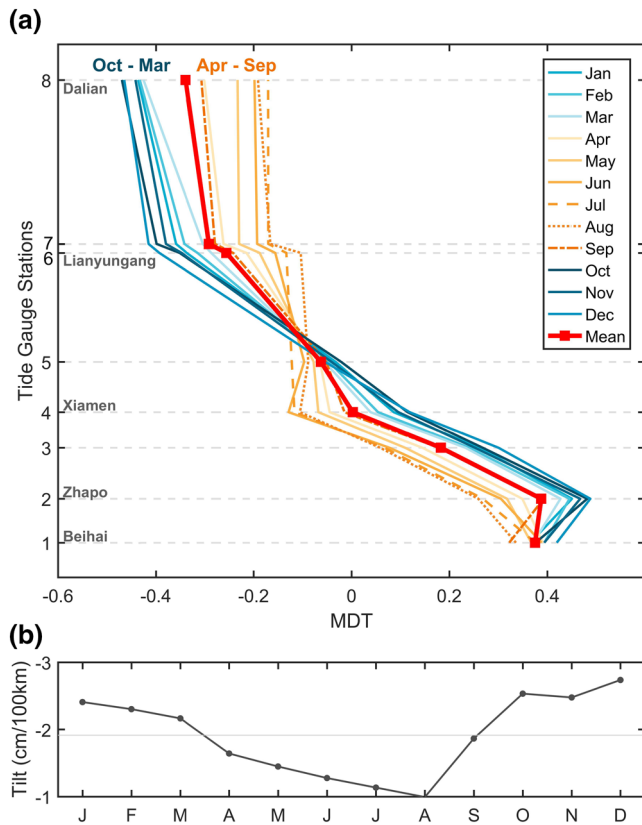


Figure 3. (a) Geodetic estimates of monthly averaged MDT (in m) profiles based on tide-gauge observations for the period of 1992–1994. The red line indicates the annual MDT, the same as the blue line in Figure 2c. (b) Monthly changes of the MDT tilt from Zhapao to Lianyungang. MDT, mean dynamic topography.

hourly National Centers for Environmental Prediction (NCEP) Climate Forecast System Reanalysis (CFSR) (Saha et al., 2010) with a horizontal resolution of 0.3125° both in longitude and latitude.

3. Results

This section first describes the characteristics of annual MDT tilt along the Chinese coast based on the geodetic and ocean approaches, and then examines the seasonality of the alongshore tilt.

3.1. Annual MDT Along the Chinese Coast

The simulated annual MDT in the China seas from HYCOM is shown in Figure 2a. The most obvious tilt feature is that the MDT in the northwestern Pacific is higher than that in the China seas, which is associated with the geostrophically balanced Kuroshio. In other words, the Kuroshio sets up the background MDT differences of $O(1)$ m between the North Pacific subtropical gyre and the China seas (e.g., Rio et al., 2014). Within the China seas, the northern MDT is obviously lower than its southern counterpart by ~ 0.7 m. Along the coastline of the Chinese mainland (see the red line in Figure 2b) of our particular interest in the present study, we calculate the alongshore MDT based on the geodetic (tide gauge) and ocean (HYCOM) approaches (Figure 2c). The comparison shows an encouraging agreement between the two profiles (red and blue lines in Figure 2c) for the period of October 1992 to September 1994. To check if the MDT averaged over the relatively short 2-year period would be biased by interannual variability, we also show the results for longer records from HYCOM (1996–2012; green line in Figure 2c) to tide gauges (1979–1995; magenta line in Figure 2c). It is clear that the profiles based on longer-term averages closely coincide with their 2-years averaged counterparts. Convergent estimates of coastal MDT from the geodetic and ocean approaches have been reported by a number of recent studies (e.g., Bingham & Haines, 2006; Higginson et al., 2015; Lin et al., 2015; Woodworth

et al., 2012). The estimated coastal MDTs all show the apparent northward drop along the coast of the Chinese mainland, consistent with the large-scale meridional MDT difference slightly offshore. The steepest tilt is found from Zhapao to Lianyungang with the tide gauge estimate of -1.92 cm per 100 km and the HYCOM estimate of -2.04 cm per 100 km. Note that the inverse barometer (IB) effect has been removed from the tide gauge records from PSMSL. The IB effect is calculated based on the formula of Wunsch and Stammer (1997) using monthly sea level pressure from the Japanese 25 years reanalysis/Japan Meteorology Agency Climate Data Assimilation System (JRA-25/JCDAS) (Onogi et al., 2007) with respect to 1013.3 hPa.

3.2. Seasonality in the Chinese Coastal MDT Tilt

Considering that the China seas undergo prominent seasonal changes in the wind forcing and coastal circulation, we now examine the seasonality in the coastal MDT tilt. Figure 3a shows the monthly averaged profiles of geodetically estimated alongshore MDT for the period of 1992–1994. Each month is corresponding to a color but the summertime (from April to September) profiles are generally labeled in oranges and the wintertime (from October to March) ones are labeled in blues. Henceforth, the summertime is defined as from April to September and the wintertime is from October to March in this study. It is evident that the MDT tilt along the Chinese coast has robust seasonal changes, with the two groups of profiles being clearly separated by the annual mean profile (red line in Figure 3a). Specifically, the alongshore profiles of MDT could be divided into four segments with different slopes of the tilt. From Beihai to Zhapao, the wintertime MDT profiles all show a northward rise, but the tilt in summer is reversed. Note that the only exception is September, which is also acceptable if being grouped to the winter season. From Zhapao to Xiamen, the MDT

profiles in all seasons exhibit a northward drop, with the tilt of -3.48 ± 0.3 cm per 100 km, which is also the steepest tilt among the four segments. Although the tilts within this segment are approximately equal with the same direction in all seasons, the driving factors could be different since the direction of the China Coastal Currents is completely reversed in winter and summer. From Xiamen to Lianyungang, MDT slopes in winter are roughly equal, tilting down toward north and steeper than those in summer. Note that the MDT tilts in July and August become almost flat or even show a mild northward rise. From Lianyungang to Dalian, the MDTs are almost flat in all seasons.

To view the seasonal variation of MDT tilt more clearly, we calculate the monthly averaged MDT tilt between Zhapo and Lianyungang where the tilt is most apparent. A clear seasonal cycle is discernable in the alongshore MDT tilt for this part of the Chinese coast (Figure 3b), with steeper tilt in winter and flatter tilt in summer. The steepest and the flattest tilts occur in December (-2.74 cm per 100 km) and in August (-0.99 cm per 100 km), respectively, and the annual mean is about -1.92 cm per 100 km (shown as gray line in Figure 3b). To check if the seasonal cycle (Figure 3b) would be affected by the relatively short period of averaging, we compare the monthly averaged MDT profiles for the period of 1992–1994 with those for the period of 1979–1995, and the seasonal cycle remains almost the same (figure not shown).

4. Momentum Budget Analysis

4.1. Alongshore Momentum Equation

The alongshore momentum equation is often used to interpret the coastal MDT tilt (Csanady, 1981; Higginson et al., 2015; Lin et al., 2015; Xu & Oey, 2011). For simplicity, we suppose the y axis to be parallel to the coast, i.e., to regard it as the alongshore coordinate. The steady, linearized, and depth-averaged alongshore momentum equation is taken to be (Csanady, 1981; Xu & Oey, 2011)

$$g\partial\eta/\partial y = \tau_{wy}/\rho_0h + \tau_{by}, \quad (1)$$

where η indicates sea surface elevation, g is acceleration due to gravity, h is water depth, τ_{wy} and τ_{by} are the alongshore components of wind stress and bottom frictional stress, respectively. The horizontal advection term is omitted because it is generally small compared to the bottom friction term, and the Coriolis term is omitted because of the assumption of no normal flow ($u = 0$ at the coast).

The term on the left-hand side of Equation 1 is the MDT tilt of our interest associated with the alongshore pressure gradient. If the bottom friction could be omitted, the MDT tilt is then balanced only by the wind forcing. So when wind blows along the y axis, sea level at the downwind side naturally rises. With the bottom friction included, the MDT tilt has to be balanced by the sum of the wind stress and bottom stress.

We integrate the individual terms of Equation 1 along the coast and thereby diagnose the contributions of alongshore wind stress (η^{τ_w}) and bottom friction (η^{τ_b}) to the alongshore variation of coastal sea level

$$\eta(y) = \eta^{\tau_w}(y) + \eta^{\tau_b}(y) \quad (2)$$

This integration of sea level components smooths out the effect of small-scale variations in bathymetry and coastline orientation, and leads to cleaner profiles that could be visualized and explained as compared with profiles calculated from individual terms in Equation 1.

4.2. Analysis of Annual MDT Tilt

According to the profiles of annual alongshore MDTs (Figure 2c), the Chinese coastal tilts are investigated at three parts: the seas north of Lianyungang, the seas from Lianyungang to Xiamen, and the seas south of Xiamen, respectively. The annual mean fields of regional sea level, surface wind, and depth-averaged currents are shown to examine their effects on the coastal tilt. Overall, the regional MDT north of Lianyungang is rather homogeneous with almost no spatial gradients of sea level, except for the slightly lower sea surface in the northwest of Bohai Sea (Figure 4a). Such a regional smooth sea level field extends to the coast, leading

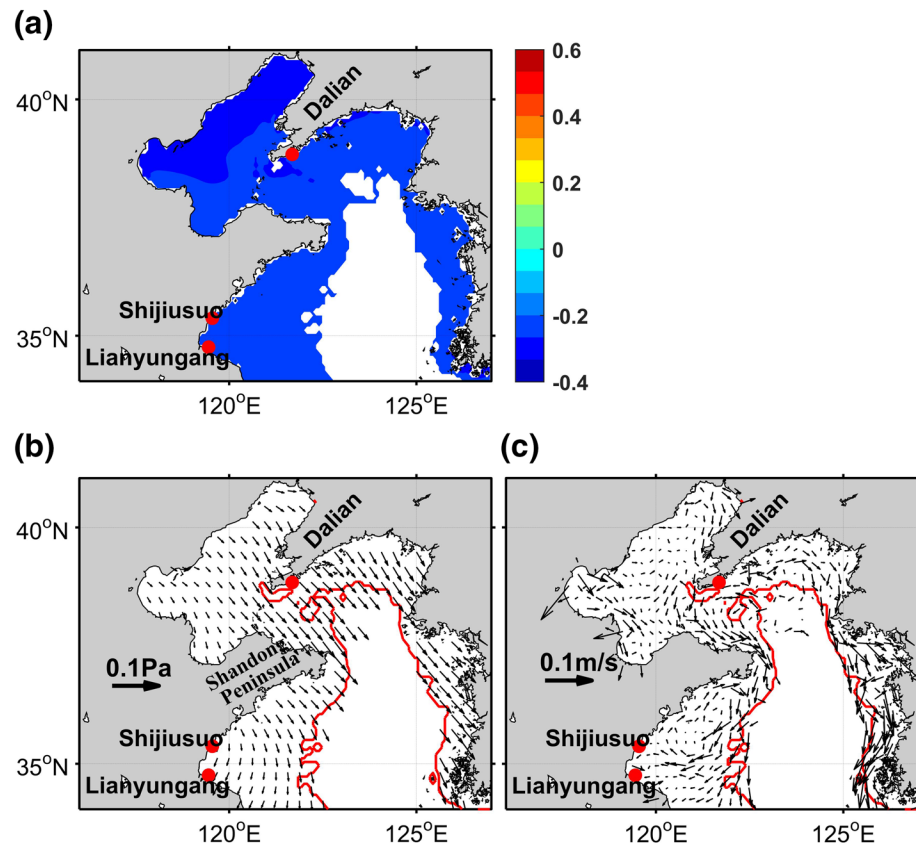


Figure 4. Annual mean fields of regional (a) sea level (in m), (b) wind stress, and (c) depth-averaged currents in the Bohai Sea and the Yellow Sea north of Lianyungang from HYCOM forcing and output for the period of October 1992 to September 1994. In (b) and (c), the red lines indicate the 50 m isobath. HYCOM, HYbrid Coordinate Ocean Model.

to the relatively flat coastal MDT at this part (Figure 2c). Mean wind stress has a relatively small magnitude of about 0.02 Pa in the Bohai Sea and the Yellow Sea, prevailing predominantly southeastward and roughly perpendicular to the coastline (Figure 4b). Such a pattern of wind field is associated with rather weak alongshore depth-averaged currents (Figure 4c), as expected from theoretical predictions (Csanady, 1981). Closer inspection suggests that the low-lying sea surface in the northwestern of Bohai Sea corresponds to even weaker coastal currents and offshore wind stress.

For the seas between Lianyungang and Xiamen (mostly in the East China Sea), the simulated annual MDT still has rather small spatial gradients over the relatively broad shelf north of 30°N whereas it has an apparently steeper alongshore tilt over the narrow shelf south of 30°N, with the sea level changes of order 0.4 m (Figure 5a). Coastal wind stress over the broad shelf is weak and approximately normal to the coast; over the narrow shelf, it is significantly stronger and mainly parallel to the coast, with a typical magnitude of 0.1 Pa (Figure 5b). The distribution of depth-averaged currents has a good correspondence to the wind stress, i.e., weaker (stronger) currents to the north (south) of 30°N (Figure 5c). Note that the current directions at the model grid points closest to the coast agree well with the wind directions, although the ones over the outer shelf show more complicated patterns. The apparent MDT tilt over the narrow shelf seems to be induced by the strong alongshore wind.

For the seas southwest of Xiamen, the annual MDT shows an apparent tilt of order 0.3 m from Xiamen to Zhao (over the northern SCS shelf); from Zhao to Beihai, nonetheless, the MDT has rather weak spatial gradients with almost flat MDT in the Beibu Gulf (Figure 6a). Mean wind stress is primarily alongshore with relatively strong magnitudes (~ 0.1 – 0.2 Pa) on the northern SCS shelf; the wind stress is weaker in the Beibu Gulf with more varying directions (Figure 6b). Again, the coastal currents correspond well with the coastal winds in terms of both magnitude and direction (Figure 6c).

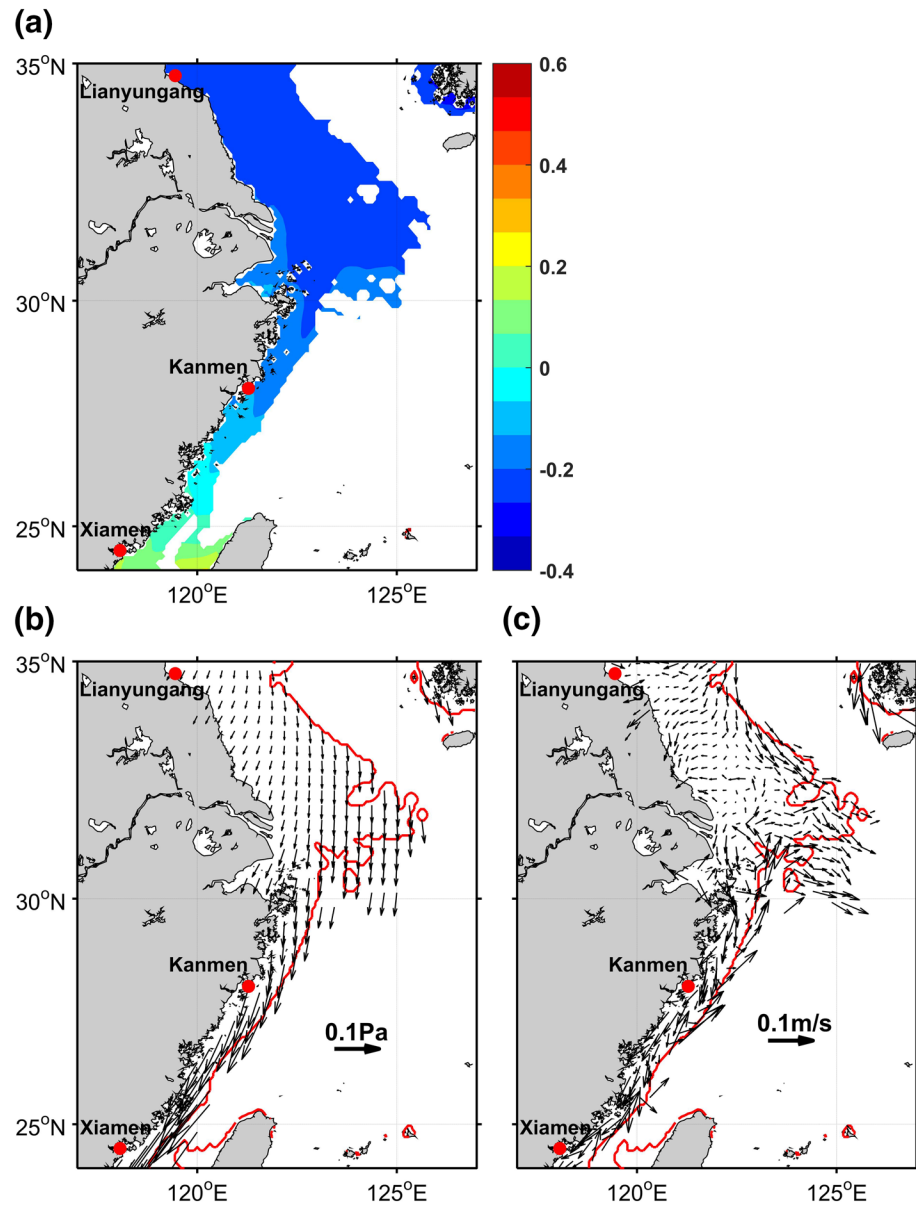


Figure 5. Same as Figure 4 but over the seas from Lianyungang to Xiamen.

In order to quantify the respective contributions of the wind stress and bottom stress to the coastal MDT tilt, we conduct the alongshore integration of Equation 1 starting from the point A (see the cyan point at one end of the red line in Figure 7a).

The contribution of the wind (η^{τ_w} , obtained by alongshore integration of $\tau_{wy} / \rho_0 g h$ at the nearest velocity point to the model coastline) shows the obvious northward drop (Figure 7b). The steepest tilt of wind contribution is detected from Lianyungang to Zhapo, in accord with the magnitude and direction of the coastal wind shown above. The range of η^{τ_w} over the entire coast reaches about 2.3 m, significantly larger than the MDT difference directly calculated by HYCOM (η) that is ~ 0.7 m.

The contribution of bottom stress, η^{τ_b} , is obtained by integrating τ_{by} alongshore. According to Wright and Thompson (1983), the time mean of alongshore bottom stress could be determined as

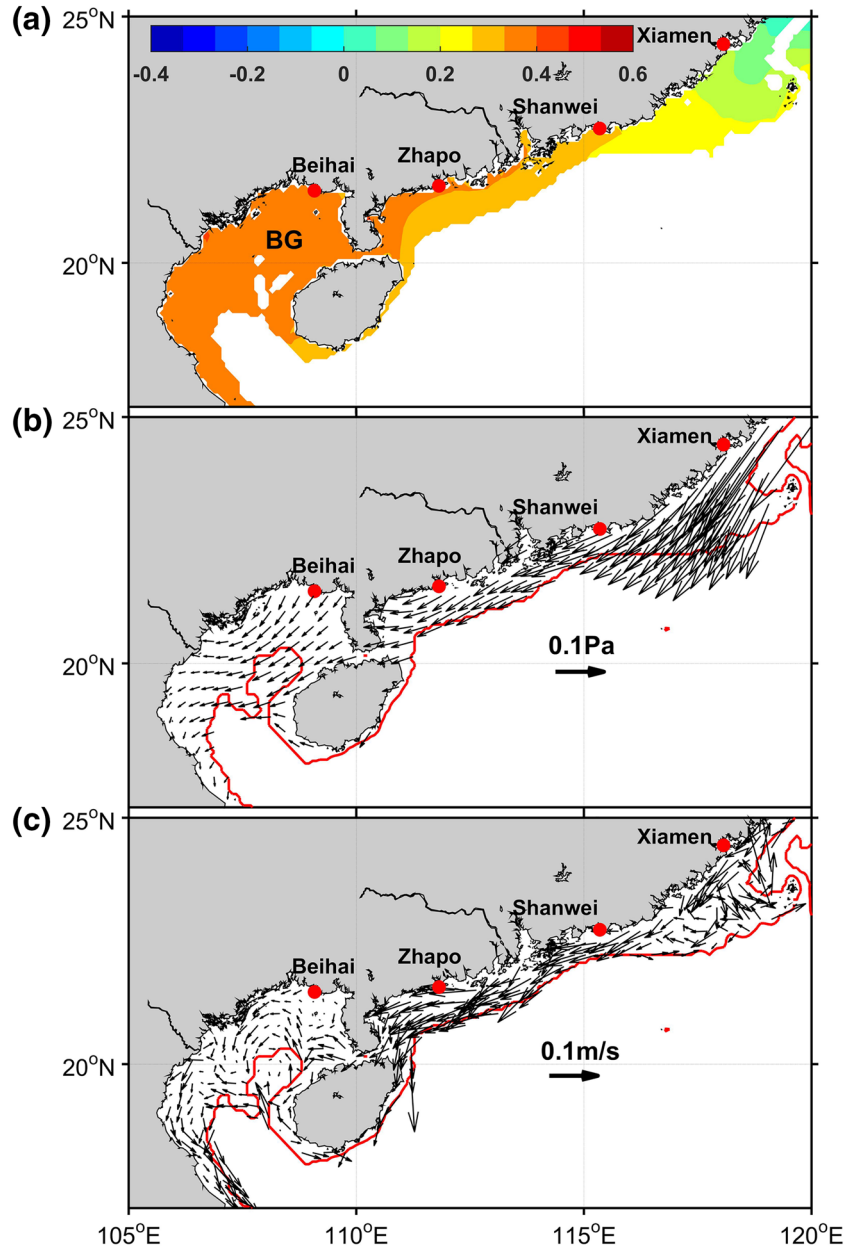


Figure 6. Same as Figure 4 but over the seas from Xiamen to Beihai. BG denotes the Beibu Gulf.

$$\tau_{by} = -\frac{c_d}{h} (v_b^2 + 4\sigma^2)^{1/2} v_b, \quad (3)$$

where c_d is the drag coefficient, v_b is the 3-hourly, depth-averaged alongshore flow, and σ is the standard deviation of the 3-hourly velocities. Following previous studies (e.g., Large & Pond, 1981; Paklar et al., 2009), we take the bottom drag coefficient of Equation 3 to be $c_d = 0.004$. The η^{tb} shows no tilt north of 30°N and an apparent northward rise south of 30°N (blue line in Figure 7b), consistent with the patterns of coastal currents shown above. The η^{tb} profile almost mirrors the changes in η^{tw} (gray line), and the sum of η^{tw} and η^{tb} closely follows the total η profile (compare the green and red lines in Figure 7b). This suggests that the annual MDT along the coast of the Chinese mainland is in fact a counter balance of the contributions from alongshore wind and bottom friction, similar to the finding of Lin et al. (2015) for the Pacific coast

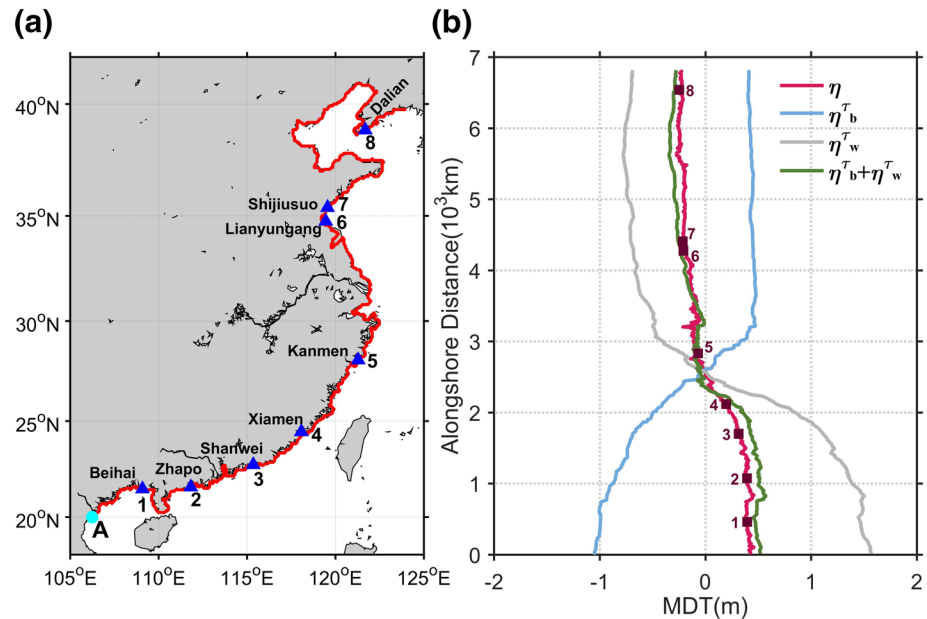


Figure 7. Momentum balance along the coast of the Chinese mainland. (a) The integration path along the coast is shown by red line. Blue triangles are the tide gauge stations. (b) Sea level components calculated from HYCOM output. The red line denotes sea level calculated directly by the model. The gray and blue lines indicate sea level contributions from wind stress and bottom friction, respectively; the green line shows their sum. HYCOM, HYbrid Coordinate Ocean Model.

of North America. The η^{τ_b} profile has a smaller range of alongshore MDT difference (~ 1.6 m) than that of η^{τ_w} (~ 2.3 m) and hence the overall alongshore MDT tilt remains a tendency of northward drop (~ 0.7 m).

4.3. Analysis of Seasonal MDT Tilt

To explain the seasonal variation of Chinese coastal MDT tilt, we first investigate the seasonality in wind stress and alongshore currents in the China seas. The winter wind stress, with a typical magnitude of 0.1 Pa, is significantly stronger than the summer wind stress, which has a magnitude of about 0.02 Pa. In winter, the seas north of Lianyungang are controlled by northwesterly wind (and mostly normal to the coast), the seas from Lianyungang to Kanmen are dominated by northerly wind, and the seas south of Kanmen are governed by northeasterly wind (Figure 8a). In summer, the seas north of Kanmen are overwhelmed by southerly wind, the seas from Kanmen to Shanwei are still dominated by relatively weak northeasterly wind, and the seas west of Shanwei are governed by southeasterly wind that is perpendicular to the coast (Figure 8b). During winter, the depth-averaged coastal currents are generally weak north of 30°N, and have a typical magnitude of 0.2 m s⁻¹ south of 30°N generally following the direction of wind stress (Figure 8c). In summer, the alongshore currents exhibit relatively complex patterns (Figure 8d). They are generally weak north of Lianyungang, similar to the wintertime coastal currents in this area. From Lianyungang to Shanwei, the summertime coastal currents are relatively strong, particularly in the Taiwan Strait (>0.2 m s⁻¹), flowing northward opposing their wintertime counterparts. The summertime coastal currents west of Shanwei are clearly weaker in magnitude (<0.05 m s⁻¹) compared to those in winter.

In order to quantify the respective contributions of the wind stress and bottom stress to the seasonal coastal MDT tilt, we also conduct the alongshore integration of Equation 1 starting from point A (the cyan point in Figure 7a). The geodetically estimated monthly climatology of MDT (based on tide gauge measurements) indicates a clear northward drop in all seasons, although the tilt in winter is sharper than that in summer (Figure 9a). The simulated monthly climatology of MDT from HYCOM closely resembles the geodetic estimates (compare Figures 9a and 9b), including the overall northward drop, steeper tilt in winter, and the position of the sharpest tilt.

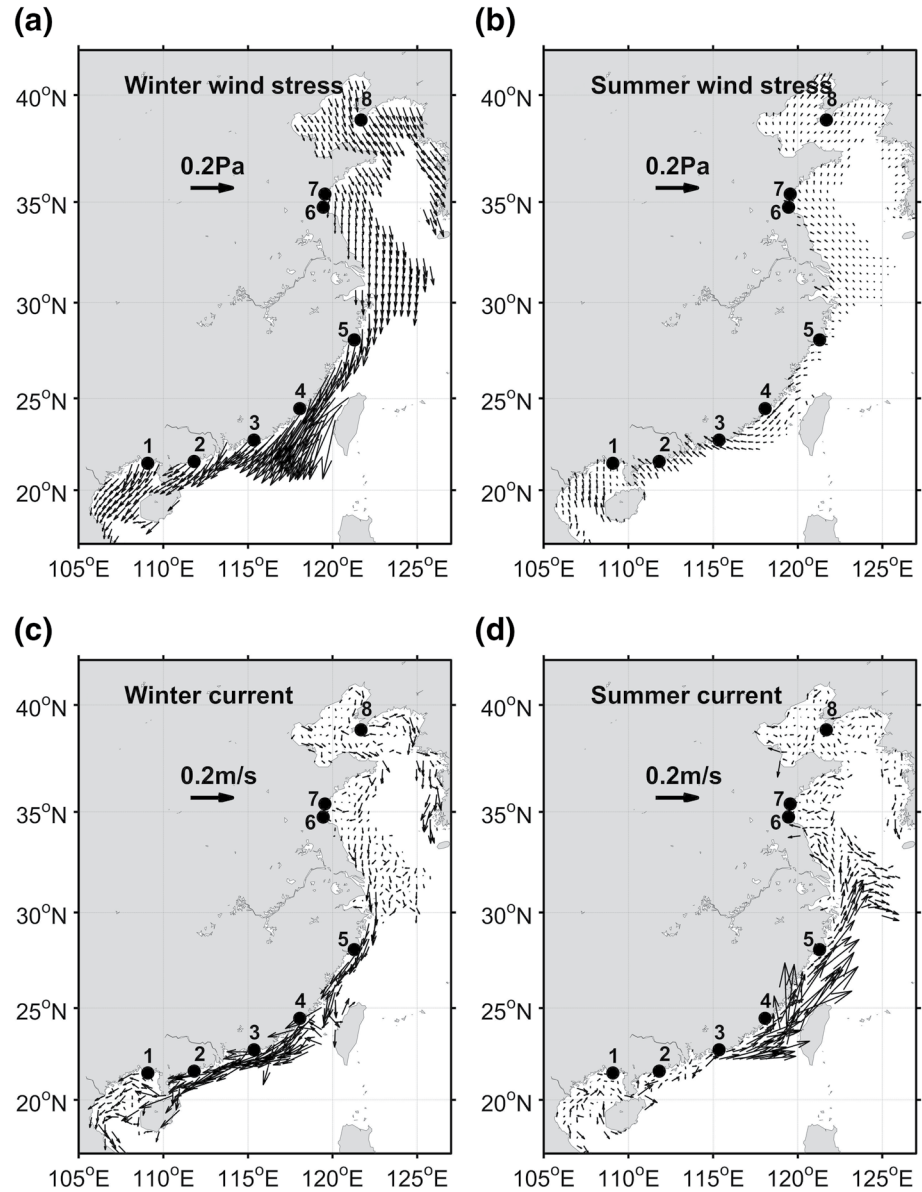


Figure 8. Spatial distributions of (upper) wind stress from NCEP CFSR and (lower) depth-averaged currents from HYCOM in (left) winter and (right) summer over the shelf of China seas. The black dots indicate the locations of the eight tide gauge stations. HYCOM, HYbrid Coordinate Ocean Model; NCEP, National Center for Environmental Prediction; CFSR, Climate Forecast System Reanalysis.

The contribution of the wind stress shows the obvious northward drop in winter, which, however, turns oppositely to a southward drop in summer (Figure 9c). This is due to the direction shifting of the alongshore winds. The reversed tilt of η^{τ_w} in summer indicates that the alongshore wind is unable to support the summertime northward drop of the total MDT seen in both geodetic and oceanographic estimates (Figures 9a and 9b). In addition, although the pattern of η^{τ_w} roughly agrees with η_{HYCOM} in winter, the magnitude of η^{τ_w} is larger than that of η_{HYCOM} by about 1 m.

The contribution of bottom stress, η^{τ_b} , is obtained by integrating τ_{by} alongshore with the same values of c_d and σ as used in Section 4.2. The monthly variation of η^{τ_b} is almost out of phase with that of η^{τ_w} , although the magnitude of η^{τ_b} is slightly smaller (Figure 9d). The pattern of η^{τ_b} resembles that of $\eta_{HYCOM} - \eta^{\tau_w}$ (compare Figures 9d and 9e), validating the calculation of η^{τ_b} itself. This suggests that the above conclusion of

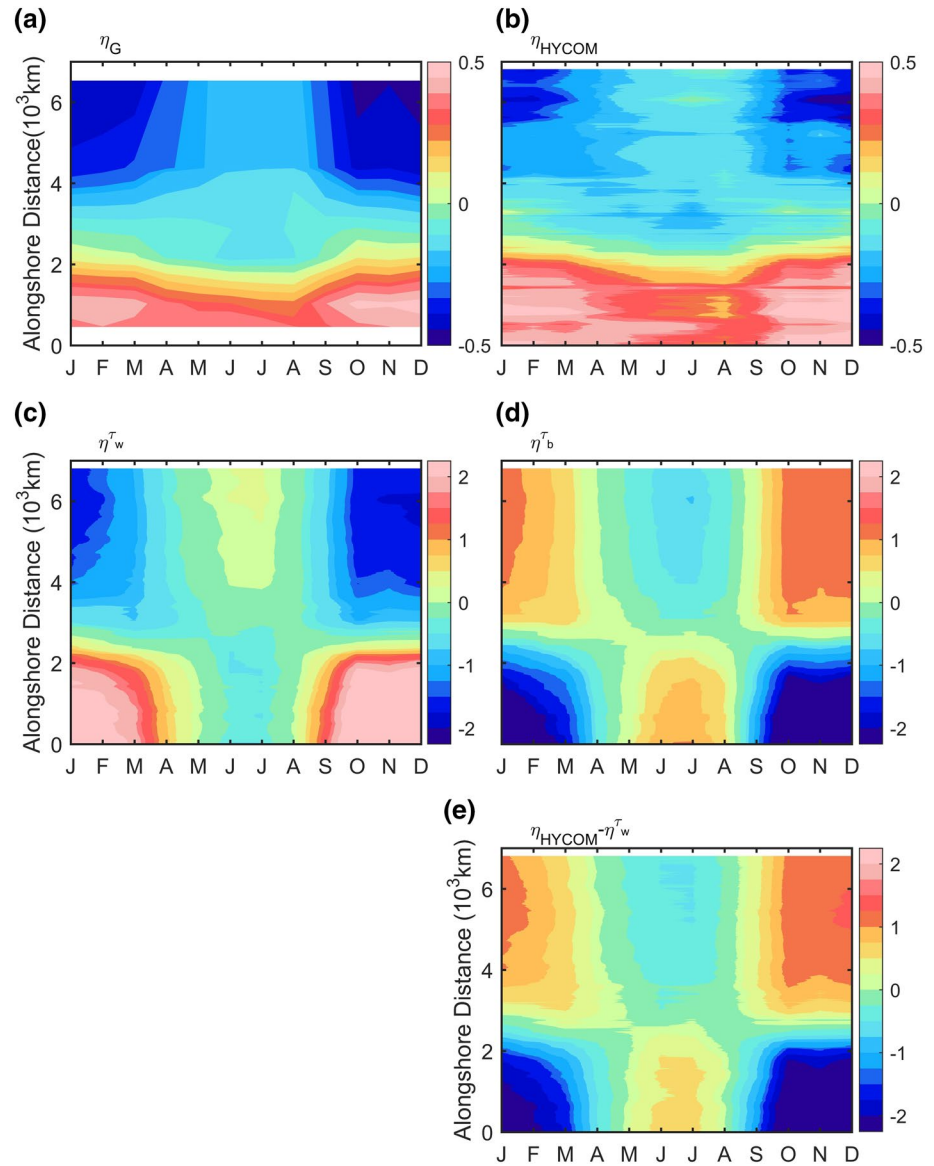


Figure 9. (a) Distance-month plot of geodetically estimated alongshore MDT (η_G ; in m) along the coast of the Chinese mainland. (b) Same as (a) but estimated from the ocean approach (η_{HYCOM} ; in m). Monthly MDT contributions from (c) alongshore wind stress (η_w^{τ} ; in m) and (d) bottom friction (η_b^{τ} ; in m). (e) The distribution of ($\eta_{HYCOM} - \eta_w^{\tau}$; in m) for comparing with η_b^{τ} in (d). Note that the color scales in (a)–(b) are different from those in (c)–(e). MDT, mean dynamic topography; HYCOM, Hybrid Coordinate Ocean Model.

the alongshore annual MDT being a counter balance of contributions from alongshore wind and bottom friction also applies to the monthly climatology of MDT, although the main contributor is different in different seasons.

Taken together, we can explain the seasonality in the MDT tilt along the coast of the Chinese mainland as follows. In winter, the coastal MDT tilt shows a northward drop, and the contribution of the strong alongshore wind stress reveals an even steeper northward drop, while the contribution of wintertime southward alongshore current reveals a northward rise. Hence, the wintertime coastal MDT tilt is mainly associated with the strong alongshore wind stress. On the other hand, due to the small contribution of alongshore wind stress, the summertime coastal MDT tilt (again northward drop) is mainly associated with the northward alongshore current. Therefore, the overall alongshore MDT tilt remains a tendency of northward drop

all year round along the coast of the Chinese mainland. With this in mind, we revisit the MDT tilt from Zhapo to Xiamen, where a northward drop with roughly equal magnitudes is observed in all months (Figure 3a). Now we understand that this northward drop is in fact mainly balanced by the alongshore wind stress in winter but by the alongshore currents in summer. We will further discuss potential mechanisms responsible for the balanced relations suggested above.

5. Discussion on Dynamic Mechanisms

The previous section suggests that the MDT tilt along the coast of the Chinese mainland is related to different contributors at different seasons, implying different dynamic mechanisms at work. When the alongshore wind is the main contributor to the coastal MDT tilt, previous studies found that the tilt could be explained by the arrested topographic wave (ATW) theory of Csanady (1978) (e.g., Hickey & Pola, 1983; Lin et al., 2015). When the coastal MDT tilt is mainly associated with coastal currents, the open-ocean forcing (e.g., large-scale winds or circulation) normally plays an important role (e.g., Liao et al., 2018; Lin et al., 2015; Yang, 2007). In this section, we will separately discuss the applicability of the ATW theory and open-ocean forcing in explaining the Chinese coastal MDT tilt.

5.1. Alongshore Wind Forcing: The Arrested Topographic Wave Theory

Considering a long and straight coastline, Csanady (1978) presented a mechanism for coastal sea level setup by the alongshore wind. The governing equations were taken to be

$$\begin{aligned} -fv &= -g \frac{\partial \zeta}{\partial x} \\ fu &= -g \frac{\partial \zeta}{\partial y} + \frac{\tau_s}{h} - \frac{\lambda v}{h} \\ \frac{\partial(uh)}{\partial x} + \frac{\partial(vh)}{\partial y} &= 0, \end{aligned} \quad (4)$$

where y axis coincides with the coast and positive x points offshore, $\zeta(x,y)$ is the surface elevation, τ_s is the alongshore (kinematic) wind stress, $u(x,y)$ and $v(x,y)$ are vertically averaged alongshore and cross-shore currents, respectively, f is the Coriolis parameter, $h(x)$ is the bottom depth assumed to be only a function of offshore distance, λ is a resistance coefficient such that λv is the bottom stress. The boundary conditions are that $uh = 0$ at the shore and $\zeta \rightarrow 0$ as $x \rightarrow +\infty$. With an inclined plane beach ($h = sx$, where $s = \text{constant}$) and periodic longshore wind stress ($\tau_s = \tau_0 \cos(ky)$, where k is the alongshore wavenumber of wind stress), surface elevation is

$$\zeta = \frac{2\tau_0}{kLgs} e^{\frac{x}{L}} \sin\left(ky + \frac{x}{L} - \frac{\pi}{4}\right) \quad (5)$$

where $L = \sqrt{2\lambda / fks}$ is the scale width of the trapped sea level in the cross-shore direction.

Invoking typical values for the study region with $f = 10^{-4} \text{ s}^{-1}$, $\tau_0 = 0.2 \times 10^{-3} \text{ m}^2 \text{ s}^{-1}$, $s = 0.003$, $\lambda = 5 \times 10^{-4} \text{ m s}^{-1}$, and $k=2\pi/4,000 \text{ km}$ (The obvious tilt is found from Beihai to Lianyungang giving an alongshore length scale of 4,000 km), we obtain the profiles of alongshore surface elevation (η), the contributions of alongshore wind stress (η^{τ_w}) and bottom stress (η^{τ_b}) based on this idealized ATW model (Figure 10). Comparing Figures 7b and 10, one can see a qualitative agreement between the predictions from ATW model and the sea level components calculated by HYCOM. The relative phases of η , η^{τ_w} , and η^{τ_b} from the ATW model agree with the HYCOM results; however, their extreme values and ranges are smaller than the profiles obtained from HYCOM. Therefore, we conclude that the alongshore wind is the major driver for the annual MDT tilt along the coast of the Chinese mainland, but it is inadequate to fully explain the details of the tilt.

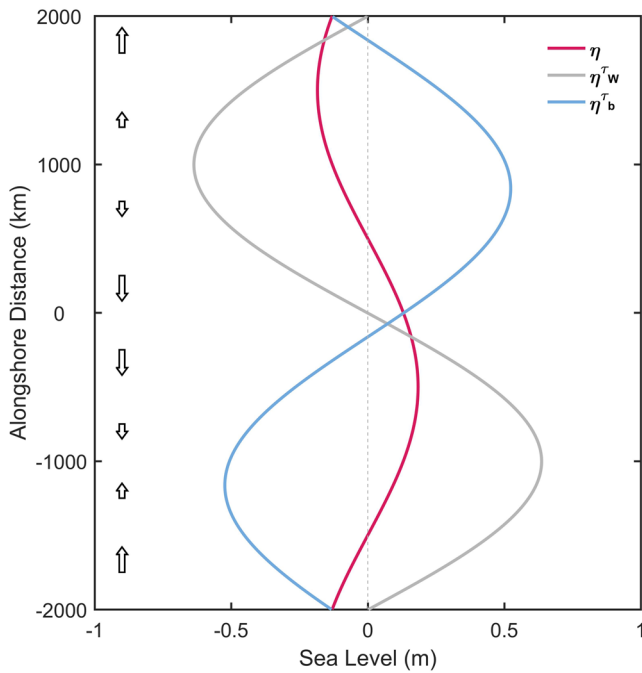


Figure 10. Alongshore sea level profiles calculated from the linear, barotropic arrested topographic wave model. The red line is the total sea level; the gray and blue lines denote contributions from the alongshore wind and bottom friction, respectively. The model is forced by the periodic wind stress. The arrows indicate the direction and magnitude of the alongshore wind stress.

The periodic alongshore wind stress could be thought of as an idealization for the realistic annual mean wind stress. However, the China seas are prevailed by the East Asia monsoon which reverses its direction from winter to summer; moreover, in each season the wind direction also varies from segment to segment along the coast of the Chinese mainland. In this case, the wind field is better idealized as a few sectors with piecewise constant alongshore wind stress in different seasons. We thus apply the Csanady (1978) ATW model by adopting the realistic piecewise alongshore wind stress, instead of the periodic one, to interpret the seasonal changes of the Chinese MDT tilts. An inclined plane beach ($h = sx$) is again assumed, and for $x = 0$

$$\zeta = -\frac{2f\tau_0}{\lambda g} \left\{ (-Ky)^{\frac{1}{2}} - [K(Y-y)]^{\frac{1}{2}} \right\} \quad (6)$$

where wind stress is prescribed for $Y > y > 0$ and zero elsewhere, $K = \lambda / (fs)$. Since the model is linear, solutions for different sectors of the coast with constant wind stress can be added together to obtain the total predicted sea surface elevation (Hickey & Pola, 1983).

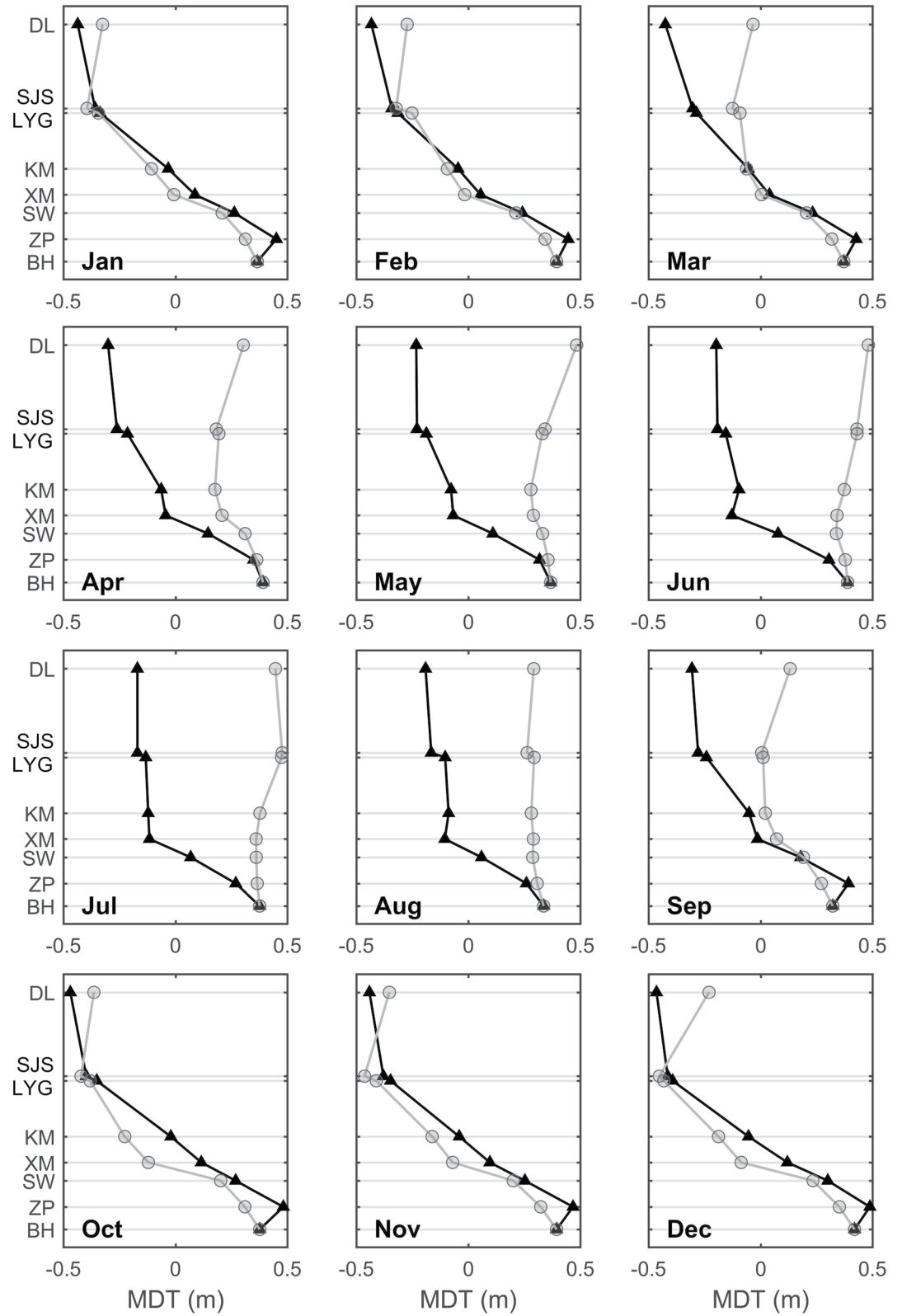
The monthly mean alongshore wind stress is from NCEP CFSR, the slope s varies from 2.5×10^{-3} south of Kanmen to 1×10^{-4} north of Lianyungang, and the coefficient of bottom friction, $\lambda = 2.5 \times 10^{-4} \text{ m s}^{-1}$, is kept constant along the coast and in time. The predictions of monthly MDT by such a model configuration have a remarkably close agreement with the observed profiles by tide gauges in winter (from October to March), including the location and range of the largest tilt (Figure 11). The agreement in summer, however, degrades dramatically, possibly because the propagation direction of the ATW signal is toward upwind rather than

downwind in summer. The degraded agreement in summer explains that the overall annual MDT predicted by ATW model agrees with the estimates obtained from HYCOM only qualitatively but not quantitatively (smaller extreme values and ranges). We thus recognize that the alongshore wind stress forcing contributes significantly to the Chinese coastal MDT tilt in winter, whereas the summertime tilt is likely related to other factors which will be discussed next.

5.2. Open-Ocean Forcing

Sturges (1974) demonstrated that certain sea-level variations along the coast of east United States were consistent with the major wind systems (trades and westerlies) and with the nature of the boundary currents. Ezer et al. (2013) and Yin and Goddard (2013) indicated that the weakening of the Gulf Stream strength would lower the sea level southeast of the Gulf Stream (in the open sea) and raise the sea level northwest of it (along the U.S. east coast), although alternative mechanisms have also been proposed (e.g., Volkov et al., 2019; Wise et al., 2020). As mentioned above, the Kuroshio sets up the background MDT difference of $O(1)$ m between the North Pacific subtropical gyre and the China seas (Figure 2a). It is likely that changes in the Kuroshio path and strength would lead to sea level changes in the China seas and possibly the sea level tilt along the Chinese coast.

To examine the influence of the Kuroshio strength on sea level distribution in the China seas, we calculate the Sverdrup transport in the subtropical North Pacific using realistic wind forcing. Since the equatorward Sverdrup transport is returned poleward via the western boundary current (Kuroshio), we could regard the magnitude of the Sverdrup transport as a surrogate for the Kuroshio strength. The Sverdrup transport, T_{Sv} , is computed by zonally integrating the wind stress curl westward from the eastern boundary



$$T_{sv}(X_W, y) = \frac{1}{\rho_0 \beta} \int_{X_E}^{X_W} \text{curl} \tau \, dX \quad (7)$$

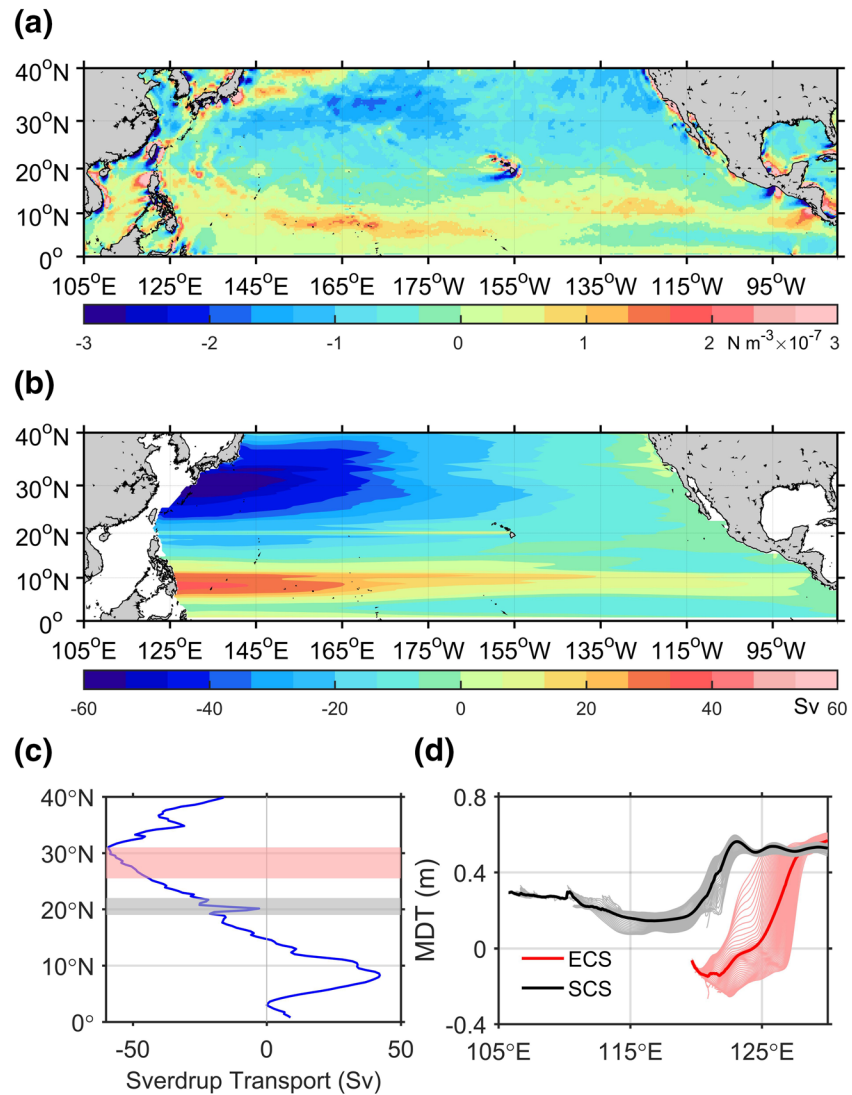


Figure 12. (a) Mean wind stress curl based on the NCEP CFSR product (October 1992 to September 1994). (b) Sverdrup transport calculated based on (a). (c) The Sverdrup transport at the western boundary. The pink and gray shadings indicate the latitudinal position of the ECS ($\sim 25.5^{\circ}\text{N}$ – 31°N) and of the SCS ($\sim 19^{\circ}\text{N}$ – 22°N). (d) The zonal MDT profiles obtained from HYCOM output within the two bands in (c). The thin lines in (d) indicate the profiles at each individual latitude, and their mean is shown by the bold lines. NCEP, National Center for Environmental Prediction; CFSR, Climate Forecast System Reanalysis; ECS, East China Sea; SCS, South China Sea; MDT, mean dynamic topography; HYCOM, HYbrid Coordinate Ocean Model.

where X and y are the zonal and meridional directions, $\rho_0 = 1,027 \text{ kg m}^{-3}$, $\beta = \partial f / \partial y$ is the meridional gradient of the Coriolis parameter, τ is the wind stress, and the X_E and X_W are the eastern boundary and western limit of integration. The mean wind stress curl is calculated from NCEP CFSR (October 1992 to September 1994), and the pattern and magnitudes (Figure 12a) are similar to those documented in the literature (e.g., Risien & Chelton, 2008). The calculated T_{Sv} reveals clear equatorward flows (negative T_{Sv}) in the subtropical gyre (Figure 12b), as expected. An interesting phenomenon is that the magnitude of T_{Sv} in the 19°N – 22°N zonal band (roughly the latitudinal position of SCS) is obviously smaller than that in the 25.5°N – 31°N zonal

Figure 11. Observed and predicted monthly MDT along the coast of the Chinese mainland. Observations are from the tide gauge measurements (black lines); predictions (gray lines) are from the Csanady (1978) ATW model forced by piecewise constant alongshore wind stress from NCEP CFSR. DL, SJS, LYG, KM, XM, SW, ZP and BH in the y axis represent Dalian, Shijiusuo, Lianyungang, Kanmen, Xiamen, Shanwei, Zhao and Beihai, respectively. MDT, mean dynamic topography; NCEP, National Center for Environmental Prediction; CFSR, Climate Forecast System Reanalysis.

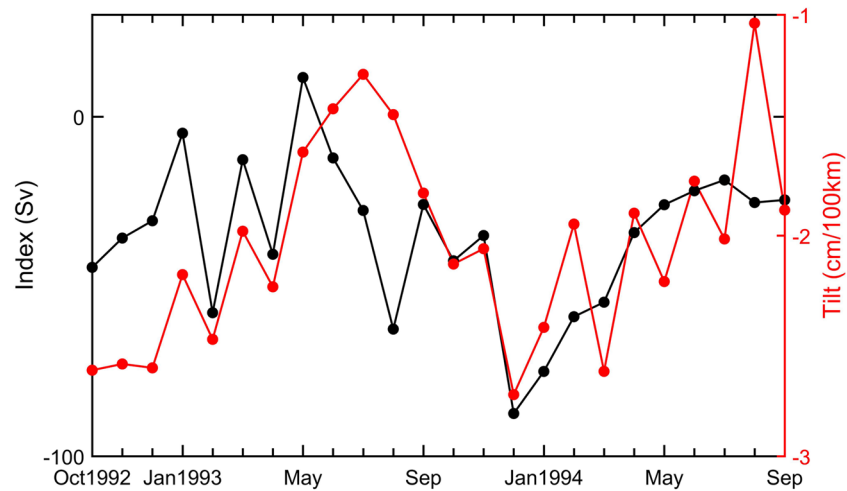


Figure 13. Monthly time series of the Kuroshio strength index (black line, in Sv) and the coastal MDT tilt (red line, in cm per 100 km) from Zhapo to Lianyungang based on the HYCOM data set. MDT, mean dynamic topography; HYCOM, HYbrid Coordinate Ocean Model.

band (roughly the latitudinal position of ECS), as shown in more detail in Figure 12c. Since the MDT on the right flank of the Kuroshio axis is approximately equal, the latitudinal difference in the Kuroshio strength, according to geostrophy, leads to higher MDT in the SCS and lower MDT in the ECS, as evidenced in Figure 12d. This explains the northward MDT drop in the offshore China seas (Figure 2a), i.e., the overall MDT decreases from the SCS to the northern seas.

The latitudinal changes in the Kuroshio strength could explain the overall northward MDT drop in the China seas, but to what extent does this open-ocean influence project to the coast? To this end, we construct an index to represent the Kuroshio strength, which is defined as the difference of T_{Sv} averaged within the region of 25.5°N–31°N and of 19°N–22°N (pink and gray shading in Figure 12c), i.e., $I = T_{Sv}^{ECS} - T_{Sv}^{SCS}$. As already shown above, the index is mostly negative. Larger magnitude of the index corresponds to larger difference in the Kuroshio strength between the vicinity of the ECS and the SCS, and to a steeper northward MDT drop in the China seas. It is intriguing to find a fairly good correspondence between the index and alongshore MDT tilt at the coastline of the Chinese mainland (Figure 13). Larger index and steeper coastal MDT tilt are seen in winter, and the opposite occurs in summer. We speculate that the open-ocean forcing (i.e., the Kuroshio strength) does affect the Chinese coastal MDT tilt, but further work is required to unravel the complex dynamics regarding on the transformation of open-ocean signals to the nearshore area.

5.3. Reconciling the Local Wind and Open-Ocean Forcing

Yang (2007) proposed that a considerable pressure gradient, governed by the western boundary layer dynamics, forces a northeastward background flow from the SCS to the ECS and persists in all seasons. According to Oey et al. (2014), the coastal currents are sensitive to the strength of alongshore wind stress: a southwestward (northeastward) flow is predicted when the wind speed is larger (smaller) than an upper (lower) bound. In other words, strong northeasterly wind in winter leads to blocking or even reversing of the northeastward current, whereas the southwesterly wind in summer results in minimal blocking or reinforcement of the background northeastward current (Jan et al., 2002). More recently, Shen et al. (2019) also indicated that a large-scale pressure gradient related to the open-ocean forcing would generate a stable northeastward flow when the winter monsoon gradually relaxes. Following this line of thought, we reconcile the alongshore wind forcing and open-ocean forcing mentioned above to interpret the MDT tilt along the coast of the Chinese mainland, in the context of the seasonally varying monsoon winds.

The abovementioned momentum balance along the coast of the Chinese mainland is mainly among the pressure gradient, wind stress, and bottom friction. In winter, the strong southwestward local wind stress dramatically reduces the northeastward background flow and even reverses it to flow southwestward in

the nearshore region of the Chinese mainland. Namely, the wind stress alone piles up water downwind to maintain the coastal MDT tilt in winter, which could also be well explained by the ATW model. When the prevailing strong southwestward wind turns to northeastward in summer, the steep coastal MDT tilt piled up in the previous winter could no longer be maintained. The tilt is thus flattened and naturally induces a return flow in the same direction of the background flow induced by the large-scale open-ocean forcing. Thus, the summer southwesterly wind ceases to dampen the northeastward background flow and even strengthens it. This explains that the summertime coastal MDT tilt is mainly maintained by the alongshore current (i.e., bottom friction).

6. Conclusions

This study examines the tilt of mean dynamic topography (MDT) along the coast of the Chinese mainland and its seasonality based on the geodetic and ocean approaches. The geodetically determined coastal MDT is estimated based on tide-gauge observations. The ocean approach directly uses the MDT output from a high-resolution ocean model, HYCOM. Estimates of the coastal MDT from the two independent approaches show a close agreement. The annual MDT along the Chinese coast shows an apparent northward drop all year round with the tide gauge-based estimate of -1.92 cm per 100 km and the HYCOM estimate of -2.04 cm per 100 km. Another key finding is that the tilt undergoes a prominent seasonal cycle. The tilt is steeper in winter but flatter in summer, with the steepest tilt of -2.74 cm per 100 km in December and the flattest one of -0.99 cm per 100 km in August, respectively, between Lianyungang and Zhapo.

Good correspondence among the mean fields of sea level, wind stress, and depth-averaged currents is found in the Chinese coastal regions. Stronger alongshore wind is associated with a larger sea level gradient in the downwind direction whereas flatter tilt accords well with weaker currents and coastal winds perpendicular to the coast. The alongshore momentum equation is used to diagnose the contributions from the alongshore wind stress and coastal currents to the coastal MDT tilt. It is found that the overall northward drop of coastal MDT along the Chinese coast is in fact a counter balance of the contributions from alongshore wind stress and bottom stress. An investigation on the seasonal changes suggests that the overall northward drop is associated primarily with the strong alongshore wind stress in winter and with coastal currents in summer, in particular for the coast between Zhapo and Xiamen.

We further demonstrate that the wintertime MDT along the Chinese coast could be well explained by the arrested topographic wave (ATW) model of Csanady (1978), which, however, could not explain the summertime coastal MDT, probably because the direction of alongshore wind stress is opposite to the propagation direction of ATW signal in summer. The summertime MDT tilt along the Chinese coast is more likely to be affected by the nearby western boundary current, Kuroshio. It is demonstrated that the latitudinal difference in the Kuroshio strength leads to the overall northward MDT drop from the SCS to the ECS, and to a northeastward background flow in all seasons. This background flow is largely blocked and reversed in winter due to the strong northeasterly monsoon, but it returns and is even intensified in summer. This offshore MDT tilt and northeastward background flow largely project to the Chinese coast, leading to the summertime northward drop in the coastal MDT.

In this study, we diagnose the coastal MDT tilts using the alongshore momentum balance by quantifying the respective contributions of local wind stress and bottom stress, and discuss the effect of local wind forcing and open-ocean forcing. The impact of topography on the coastal tilt is largely omitted here. As discussed by Jan et al. (2002), the local topography, together with the monsoon, leads to the blocking of northward current in the Taiwan Strait. Oey et al. (2014) showed that the cross-strait flow would be amplified by the stationary Rossby wave formed downstream of a topographic ridge off midwestern Taiwan. Nonetheless, such topographic effect is more manifested in the local circulation, associated with local sea-level slopes (Shen et al., 2019). We note that the large-scale pressure gradient along the entire coast of the Chinese mainland is related more significantly to the continental shelf/slope. It is also worth noting that the open-ocean signals do not merely transform to a reduced-amplitude version when approaching the coast; they are largely inhibited by the continental slope (Brink, 1998; Huthnance, 2004). Hughes et al. (2019) indicated that the coastal trapped waves advect sea level signals rapidly along the continental slopes, but diffuse the signals slowly across the slope due to bottom friction. Hence, further investigations are required in the next

step to unravel the relationship between the deep-ocean signals and coastal sea level in the vicinity of China seas which are featured by complex topography.

Acknowledgments

This study was supported by the National Natural Science Foundation of China (Nos. 91958203, 91858201, 42076013, 41730533, 41890801, and 41606009), the Natural Science Foundation of Fujian Province of China (No. 2019J05009), and Xiamen University Fundamental Research Funds for the Central Universities (No. 20720180099). The tide gauge data are obtained from the Permanent Service for Mean Sea Level (PSMSL; <https://www.psmsl.org/>). The output from the HYbrid Coordinate Ocean Model (HYCOM) is available online (<https://www.hycom.org/data/glbUpt08/expt-19pt0>). The hourly wind data from the National Centers of Environmental Prediction (NCEP) Climate Forecast System Reanalysis (CFRS) are downloaded from <https://www.ncdc.noaa.gov/data-access/model-data/model-datasets/climate-forecast-system-version2-cfsv2#CFS> Reanalysis (CFRS). The sea level pressure from JRA-25/JCDAS is available online (<http://apdrc.soest.hawaii.edu/datadoc/jra25mp.php>). We appreciate comments from the Editor and three anonymous reviewers that have improved early versions of the manuscript. We also thank the *Young Scientist Forum on Ocean Dynamics* for insightful discussions on certain aspects of the present study.

References

Bingham, R. J., & Haines, K. (2006). Mean dynamic topography: intercomparisons and errors. *Philosophical Transactions of the Royal Society A: Mathematical, Physical and Engineering Sciences*, 364(1841), 903–916.

Brink, K. H. (1998). Deep-sea forcing and exchange processes. In K. H. Brink & A. R. Robinson (Eds.), *The Sea, Ideas and Observations on Progress in the Study of the Seas* (Vol. 10, pp. 151–167). New York, NY: John Wiley and Sons.

Chen, X. Y., Hao, Z. Z., Pan, D. L., Huang, S. X., Gong, F., & Shi, D. S. (2014). Analysis of temporal and spatial feature of sea surface wind filed in China offshore. *Journal of Marine Sciences*, 32(1), 1–10 (in Chinese).

Csanady, G. T. (1978). The arrested topographic wave. *Journal of Physical Oceanography*, 8, 47–62. [https://doi.org/10.1175/1520-0485\(1978\)08<0047:TATW.2.CO;2](https://doi.org/10.1175/1520-0485(1978)08<0047:TATW.2.CO;2)

Csanady, G. T. (1981). Circulation in the coastal ocean. *Advances in geophysics*, 23, 101–183. [https://doi.org/10.1016/S0065-2687\(08\)60331-3](https://doi.org/10.1016/S0065-2687(08)60331-3)

Cummings, J. A., & Smedstad, O. M. (2013). Variational Data Assimilation for the Global Ocean. In S. Park & L. Xu (Eds.), *Data Assimilation for Atmospheric, Oceanic and Hydrologic Applications* (Vol. II, pp. 303–343). Heidelberg, Berlin: Springer. https://doi.org/10.1007/978-3-642-35088-7_13

Ezer, T., Atkinson, L. P., Corlett, W. B., & Blanco, J. L. (2013). Gulf Stream's induced sea level rise and variability along the U.S. mid-Atlantic coast. *Journal of Geophysical Research: Oceans*, 118, 685–697. <https://doi.org/10.1002/jgrc.20091>

Featherstone, W. E., & Filmer, M. S. (2012). The north-south tilt in the Australian height datum is explained by the ocean's mean dynamic topography. *Journal of Geophysical Research*, 117, C08035. <https://doi.org/10.1029/2012JC007974>

Feng, H. J., Gu, D. S., Zhang, L., et al. (1998). The research on the Earth crust vertical movement characteristic and mechanism in eastern China. *Acta Geodaetica et Cartographica Sinica*, 1, 16–23 (in Chinese).

Gordon, A. L., Huber, B. A., Metzger, E. J., Susanto, R. D., Hurlburt, H. E., & Adi, T. R. (2012). South China Sea throughflow impact on the Indonesian throughflow. *Geophysical Research Letters*, 39, L11602. <https://doi.org/10.1029/2012GL052021>

Hickey, B. M., & Pola, N. E. (1983). The seasonal alongshore pressure gradient on the west coast of the United States. *Journal of Geophysical Research*, 88(C12), 7623–7633.

Higginson, S., Thompson, K. R., Woodworth, P. L., & Hughes, C. W. (2015). The tilt of mean sea level along the east coast of North America. *Geophysical Research Letters*, 42, 1471–1479. <https://doi.org/10.1002/2015GL063186>

Huang, J. (2017). Determining coastal mean dynamic topography by geodetic methods. *Geophysical Research Letters*, 44(21), 11–125.

Hughes, C. W., Fukumori, I., Griffies, S. M., Huthnance, J. M., Minobe, S., Spence, P., & (2019). Sea Level and the Role of Coastal Trapped Waves in Mediating the Influence of the Open Ocean on the Coast. *Surveys in Geophysics*, 40, 1467–1492.

Huthnance, J. M. (2004). Ocean-to-shelf signal transmission: A parameter study. *Journal of Geophysical Research*, 109, C12029. <https://doi.org/10.1029/2004JC002358>

Hu, J., & Wang, X. H. (2016). Progress on upwelling studies in the China seas. *Reviews of Geophysics*, 54(3), 653–673.

Jan, S., Wang, J., Chern, C.-S., & Chao, S.-Y. (2002). Seasonal variation of the circulation in the Taiwan Strait. *Journal of Marine Systems*, 35, 249–268.

Jia, Y., Zhang, Y., & Lin, M. (2013). The numerical simulation of the Kuroshio frontal eddies in the East China Sea using a hybrid coordinate ocean mode. *Acta Oceanologica Sinica*, 32(5), 31–41.

Kuroishi, Y. (2013). Comparison of latest global and regional gravimetric geoid models with GPS/leveling geoidal undulations over Japan. *Reference Frames for Applications in Geosciences* (pp. 221–227). Berlin, Heidelberg: Springer.

Large, W. G., & Pond, S. (1981). Open ocean momentum flux measurements in moderate to strong winds. *Journal of Physical Oceanography*, 11(3), 324–336.

Lau, K. M., & Li, M. T. (1984). The monsoon of East Asia and its global associations-A survey. *Bulletin of the American Meteorological Society*, 65(2), 114–125.

Liao, E., Oey, L., Yan, X., Li, L., & Jiang, Y. (2018). The deflection of the China Coastal Current over the Taiwan Bank in winter. *Journal of Physical Oceanography*, 48(7), 1433–1450. <https://doi.org/10.1175/JPO-D-17-0037.1>

Lin, H., Thompson, K. R., Huang, J., & Véronneau, M. (2015). Tilt of mean sea level along the Pacific coasts of North America and Japan. *Journal of Geophysical Research: Oceans*, 120(10), 6815–6828.

McCabe, R. M., Hickey, B. M., Dever, E. P., & MacCready, P. (2015). Seasonal cross-shelf flow structure, upwelling relaxation, and the alongshelf pressure gradient in the northern California Current System. *Journal of Physical Oceanography*, 45, 209–227. <https://doi.org/10.1175/JPO-D-14-0025.1>

Naimie, C. E., Blain, C. A., & Lynch, D. R. (2001). Seasonal mean circulation in the Yellow Sea—a model-generated climatology. *Continental Shelf Research*, 21(6-7), 667–695.

Oey, L. Y., Chang, Y. L., Lin, Y. C., Chang, M. C., Varlamov, S., & Miyazawa, Y. (2014). Cross flows in the Taiwan Strait in winter. *Journal of Physical Oceanography*, 44, 801–817.

Onogi, K., Tsutsui, J., Koide, H., Sakamoto, M., Kobayashi, S., Hatsushika, H., et al. (2007). The JRA-25 reanalysis. *Journal of the Meteorological Society of Japan*, 85, 369–432.

Paklar, G. B., Koraćin, D., & Dorman, C. (2009). Wind-induced ocean circulation along California and Baja California coasts in June 1999. *Atmospheric Research*, 94(1), 106–133.

Park, J.-H., & Farmer, D. (2013). Effects of Kuroshio intrusions on nonlinear internal waves in the South China Sea during winter. *Journal of Geophysical Research: Oceans*, 118, 7081–7094. <https://doi.org/10.1002/2013JC008983>

Penna, N. T., Featherstone, W. E., Gazeaux, J., & Bingham, R. J. (2013). The apparent British sea slope is caused by systematic errors in the levelling-based vertical datum. *Geophysical Journal International*, 194(2), 772–786.

Reid, J. L., & Mantyla, A. W. (1976). The effect of the geostrophic flow upon coastal sea elevations in the northern North Pacific Ocean. *Journal of Geophysical Research*, 81, 3100–3110.

Rio, M. H., Mulet, S., & Picot, N. (2014). Beyond GOCE for the ocean circulation estimate: Synergetic use of altimetry, gravimetry, and in situ data provides new insight into geostrophic and Ekman currents. *Geophysical Research Letters*, 41(24), 8918–8925.

Risien, C. M., & Chelton, D. B. (2008). A Global Climatology of Surface Wind and Wind Stress Fields from Eight Years of QuikSCAT Scatterometer Data. *Journal of Physical Oceanography*, 38, 2379–2413. <https://doi.org/10.1175/2008JPO3881.1>

- Saha, S., Moorthi, S., Pan, H. L., et al. (2010). The NCEP climate forecast system reanalysis. *Bulletin of the American Meteorological Society*, 91(8), 1015–1058.
- Shen, J., Zhang, J., Qiu, Y., Li, L., & Jing, C. (2019). Winter counter-wind current in western Taiwan Strait: characteristics and mechanisms. *Continental Shelf Research*, 172, 1–11.
- Stommel, H., & Leetmaa, A. (1972). Circulation on the continental shelf. *Proceedings of the National Academy of Sciences of the United States of America*, 69(11), 3380–3384. <https://doi.org/10.1073/pnas.69.11.3380>
- Sturges, W. (1974). Sea level slope along continental boundaries. *Journal of Geophysical Research*, 79(6), 825–830.
- Tomczak, M., & Godfrey, J. S. (1994). Adjacent seas of the Pacific Ocean. *Regional oceanography: an introduction*. Elsevier.173191 <https://doi.org/10.1016/B978-0-08-041021-0.50014-X>
- Volkov, D. L., Lee, S.-K., Domingues, R., Zhang, H., & Goes, M. (2019). Interannual sea level variability along the southeastern seaboard of the United States in relation to the gyre-scale heat divergence in the North Atlantic. *Geophysical Research Letters*, 46, 7481–7490. <https://doi.org/10.1029/2019GL083596>
- Werner, F. E., & Hickey, B. M. (1983). The role of a longshore pressure gradient in Pacific Northwest coastal dynamics. *Journal of Physical Oceanography*, 13, 395–410. [https://doi.org/10.1175/1520-0485\(1983\)013<0395:TROALP.2.CO;2](https://doi.org/10.1175/1520-0485(1983)013<0395:TROALP.2.CO;2)
- Wise, A., Polton, J. A., Hughes, C. W., & Huthnance, J. M. (2020). Idealised modelling of offshore-forced sea level hot spots and boundary waves along the North American East Coast. *Ocean Modelling*, 155 <https://doi.org/10.1016/j.ocemod.2020.101706>
- Woodworth, P. L., & Player, R. (2003). The permanent service for mean sea level: an update to the 21st Century. *Journal of Coastal Research*, 19(2), 287–295.
- Woodworth, P. L., Hughes, C. W., Bingham, R. J., & Gruber, T. (2012). Towards worldwide height system unification using ocean information. *Journal of Geodetic Science*, 2(4), 302–318.
- Wright, D. G., & Thompson, K. R. (1983). Time-averaged forms of the nonlinear stress law. *Journal of Physical Oceanography*, 13(2), 341–345.
- Wunsch, C., & Stammer, D. (1997). Atmospheric loading and the oceanic “inverted barometer” effect. *Reviews of Geophysics*, 35(1), 79–107. <https://doi.org/10.1029/96RG03037>
- Xu, F.-H., & Oey, L.-Y. (2011). The origin of along-shelf pressure gradient in the Middle Atlantic Bight. *Journal of Physical Oceanography*, 41(9), 1720–1740. <https://doi.org/10.1175/2011JPO4589.1>
- Yang, J. Y. (2007). An oceanic current against the wind: how does Taiwan Island steer warm water into the East China Sea?. *Journal of Physical Oceanography*, 37, 2563–2569.
- Yang, Y., Li, K., Du, J., Liu, Y., Liu, L., Wang, H., & Yu, W. (2019). Revealing the subsurface Yellow Sea Cold Water Mass from satellite data associated with Typhoon Muifa. *Journal of Geophysical Research: Oceans*, 124, 7135–7152. <https://doi.org/10.1029/2018JC014727>
- Yin, J., & Goddard, P. B. (2013). Oceanic control of sea level rise patterns along the East Coast of the United States. *Geophysical Research Letters*, 40(20), 5514–5520.
- Yu, Z., Metzger, E. J., Thoppil, P., Hurlburt, H. E., Zamudio, L., Smedstad, O. M., et al. (2015). Seasonal cycle of volume transport through Kerama Gap revealed by a 20-year global HYbrid Coordinate Ocean Model reanalysis. *Ocean Modelling*, 96, 203–213.
- Yu, Z. K., Gao, J. Y., & Wu, X. L. (1989). Difference between mean sea level and National Geoid (1985) along the coast of China. *Journal of Oceanography In Taiwan Strait*, 8(2), 97–104 (in Chinese).
- Zhai, G. J., Zhao, M. C., & Huang, M. T. (1993). Computation and Study of the SST in Chinese Coastal Waters. *Advances In Water Science*, 4(3), 161–170 (in Chinese).
- Zhang, C. J. (2002). The sea level slope along China's coast of the Northwest Pacific and its primary research on mechanism. *Acta Oceanologica Sinica*, 24(5), 19–25 (in Chinese).
- Zhao, M. C., & Han, X. H. (1990). China Offshore Sea-surface Topography and Qingdao Station Elevation Datum's Difference. *Marine Science Bulletin*, 9(2), 15–22 (in Chinese).